

Deep Imaging of Diffuse Light Around Galaxies and Clusters: Progress and Challenges

J. Christopher Mihos¹

¹Department of Astronomy
Case Western Reserve University
10900 Euclid Ave, Cleveland OH, USA
email: mihos@case.edu

Abstract. Over the past several decades, advances in telescope/detector technologies and deep imaging techniques have pushed surface brightness limits to ever fainter levels. We can now both detect and measure the diffuse, extended star light that surrounds galaxies and permeates galaxy clusters, enabling the study of galaxy halos, tidal streams, diffuse galaxy populations, and the assembly history of galaxies and galaxy clusters. With successes come new challenges, however, and pushing even deeper will require careful attention to systematic sources of error. In this review I highlight recent advances in the study of diffuse starlight in galaxies, and discuss challenges faced by the next generation of deep imaging campaigns.

Keywords. galaxies: general, galaxies: clusters: general, telescopes, surveys

1. Introduction

While much attention has been focused on extreme low surface brightness (LSB) science[†] in recent years, the field itself is hardly new. As far back as eighty five years ago, [Stebbins & Whitford \(1934\)](#) were using a photoelectric photometer on the Mt Wilson 100" telescope to trace M31's surface brightness profile down to $\mu_{pg} \approx 26 - 27$ mag arcsec⁻², while by the 1950s Zwicky was already postulating the existence of intracluster light (ICL) based on imaging of tidal streams around cluster galaxies ([Zwicky 1952](#)). Indeed, many of the scientific issues this conference focuses on have been motivated by deep imaging studies in the 1970s and 1980s. Deep photographic imaging revealed the structure and color of the extended envelopes of bright ellipticals (e.g., [Arp & Bertola 1969](#); [de Vaucouleurs 1969](#)), and showed a myriad of stellar shells and streams marking the accretion of material onto spiral and elliptical galaxies (e.g., [Malin & Carter 1980](#); [Schweizer & Seitzer 1988](#)). On larger scales, the diffuse ICL in Coma was first imaged in the early 1970s ([de Vaucouleurs, & de Vaucouleurs 1970](#); [Welch & Sastry 1971](#)), while deep surveys of Virgo in the 1980s had already uncovered a population of large and extremely diffuse galaxies throughout the cluster ([Sandage & Binggeli 1984](#)).

In the years since these discoveries, advances in telescope technology, instrumentation, and data analysis have allowed astronomers to survey the low surface brightness universe down to even greater depths and over wider areas than previously possible. Modern imaging that carefully corrects for (or mitigates) contamination due to stray light and astronomical foregrounds and backgrounds can reach down to optical surface brightnesses as low as 29–30 mag arcsec⁻² — and even lower in certain cases. We have now moved beyond simple detection of LSB features and into the realm of accurate photometric studies

[†] Here I rather arbitrarily define “extreme LSB” as optical surface brightnesses at or below 1% of the ground-based night sky brightness, or $\mu_V \gtrsim 26 - 27$ mag arcsec⁻².

of the structure and stellar populations that compose the diffuse starlight surrounding galaxies.

Deep LSB imaging of galaxies and clusters is particularly important given the information held in the low surface brightness structure that surrounds them. The dynamical timescales are long in galaxy outskirts, such that the faint tidal streams and shells from past interactions and accretion events may survive for many Gyr. The morphologies, colors, and kinematics of tidal tails provide important constraints on the dynamical evolution of interacting galaxies. Deep imaging can also reveal the structure of diffuse galaxy halos and the history of satellite accretion in galaxies. On the largest scales, the diffuse intracluster light (ICL) that permeates massive galaxy clusters can be used to trace cluster assembly history. The key requirement, though, is to go deep: it is at the lowest surface brightnesses ($\gtrsim 28\text{--}30\text{ mag arcsec}^{-2}$) that galaxy halos are predicted to be awash in accretion streams, and where the diffuse light in clusters decouples from the galaxy outskirts and instead traces the complex accretion structure of the intracluster light.

2. Deep Imaging: Depths and Strategies

Before embarking on an overview of LSB imaging studies, it is important to recognize that, unlike point source depths, there is no well-defined metric for surface brightness depth; this has led to different groups quantifying depths in different ways. Complicating matters is the fact that some studies report limiting depths in terms of derived quantities: surface brightnesses of detected objects, limits to surface brightness or color profiles, etc. Comparisons such as these conflate the quality of the *data* and the depth of the *analysis*. Even the most straight-forward metric — the background variation in the imaging measured over a fixed spatial scale (e.g. Trujillo & Fliri 2016; Mihos et al. 2017) — is not uniquely defined, as it employs a scale that will necessarily differ depending on the characteristics of the telescope and detector. For example, *Hubble ACS* imaging has $0.05''$ pixels and a $202'' \times 202''$ FOV, while small ground-based telescopes have arcsecond-scale pixels and degree-scale FOVs. When both the pixel scale and areal coverage differ by more than an order of magnitude between two datasets, a direct statistical comparison of the background fluctuations on fixed angular scale is ill-posed, and ultimately not well-motivated. The scientific goals of such projects are typically quite different, as *Hubble* studies of diffuse light have focused on higher redshift systems with small angular scale, while LSB imaging of nearby galaxies has been the province of ground-based observatories with wide-field capabilities.

In addition, if the goal is to go uniformly deep over a wide area, metrics should also quantify both the limiting depth and its variation over large angular scales, a practice that is rarely done. Here too, however, singular definitions can be problematic. Studies that search for small-scale diffuse features (LSB galaxies or tidal streams around distant objects) can tolerate large-scale variations in depth as long as a local background can be accurately modeled. In contrast, when studying the extended halos of nearby galaxy or diffuse light in clusters, the imaging *must* be very uniform over much larger scales. All these issues make direct comparisons of published depths quite difficult.† As a result, in this review I make no attempt to “standardize” depths to a single unique metric, but instead give the limiting depths as reported by different surveys, highlighting the angular

† The task is made even *more* difficult by sometimes hyper-competitive focus on being “The Deepest.” This has led to claims of limiting depths which are often over-stated, or the use of improper comparison metrics cherry-picked to advantage a particular study. This practice distorts the science and is harmful to the field.

scale and statistical metric used whenever possible. Ultimately I leave the reader with one final warning when interpreting limiting depths: *caveat emptor*.

Over the past years, a variety of deep imaging projects have come online which employ different strategies to probe the low surface brightness universe. One approach uses small telescopes or telescope arrays optimized for low surface brightness imaging. Such systems are competitive even in the world of large telescopes, as photometric errors in deep surface photometry are dominated not by photon statistics but by systematic sources of uncertainty due to flat-fielding variations, sky and background estimation, and contamination by stray light. This latter issue is perhaps the most problematic, and arises from a variety of sources including the extended wings of the PSF, extraneous off-axis light, scattered light within the telescope, reflections between various optical elements, and complex diffraction patterns from obstructions in the telescope beam. Thus, systems which mediate these effects through optical design choices (using closed tube telescopes or telescopes with unobstructed beams, reducing the number of reflective surfaces, employing aggressive anti-reflective coatings, etc) can provide significant advantages. Furthermore, for surface photometry, the fast beams and large pixel scales of these systems provide additional benefits: more photons per pixel to estimate sky backgrounds and reduce photon noise, and the ability to image large fields of view without the need for CCD arrays and the chip-to-chip sensitivity variations they introduce. Examples of these types of telescopes include the LSB-optimized Burrell Schmidt telescope (Mihos et al. 2017) reaching limiting depths of $\mu_{B,lim} \approx 29.5$ mag arcsec⁻² ($3\sigma, 1'$ scales), and the Dragonfly imaging array (Abraham & van Dokkum 2014) which reaches a comparable depth of $\mu_{g,lim} \approx 29.5$ mag arcsec⁻² ($1\sigma, 1'$ scales; Merritt et al. 2016).

Of course larger telescopes deliver significant advantages of their own, most obviously in their collecting area but also in finer pixel scale. This provides not only more photons and better spatial resolution, but the ability to better resolve and mask out stars and background galaxies that would otherwise contaminate the surface photometry. Large telescopes equipped with large format CCD arrays can now image over a wide area, albeit often at the cost of increased scattered light from correcting optics and/or complicated sensitivity variations across the array. These tradeoffs are illustrated in Figure 1, which compares deep imaging of the Virgo giant elliptical M49 using the 0.6/0.9m Burrell Schmidt telescope (Janowiecki et al. 2010) to that taken with Megacam on the 3.6m CFHT telescope (Arrigoni Battaia et al. 2012). The center panels show the raw imaging data, with the top insets showing a $2'$ zoom of a portion of the field. Compared to the Burrell Schmidt imaging, the superior resolution and point source depth of the CFHT data is clear. The bottom panels shows the result after subtracting smooth models for M49's light, masking compact sources, and median-binning the images spatially to highlight M49's diffuse shell system. In the CFHT imaging, the higher spatial resolution and better masking of contaminants leads to a smoother, more detailed map of the shells on small scales. However, on larger scales chip-to-chip variations in sensitivity can be seen as linear artifacts in the residual image, along with circular reflections from bright stars in the field. In contrast, the Burrell Schmidt imaging is more uniform on large scales, due to its single CCD detector and use of aggressive anti-reflection coatings on the optical elements of the camera.

Deep targeted surveys using 3m-class telescopes have studied nearby galaxies and clusters, including the *Next Generation Virgo Cluster Survey* (Ferrarese et al. 2012) and ATLAS3D survey (Cappellari et al. 2011) on CFHT, and the *Fornax Deep Survey* (Iodice et al. 2016) and VEGAS survey (Capaccioli et al. 2015) on the VST telescope at ESO. While these telescopes are not specifically optimized for LSB science, through careful reduction techniques these surveys have typically achieved limiting surface brightnesses

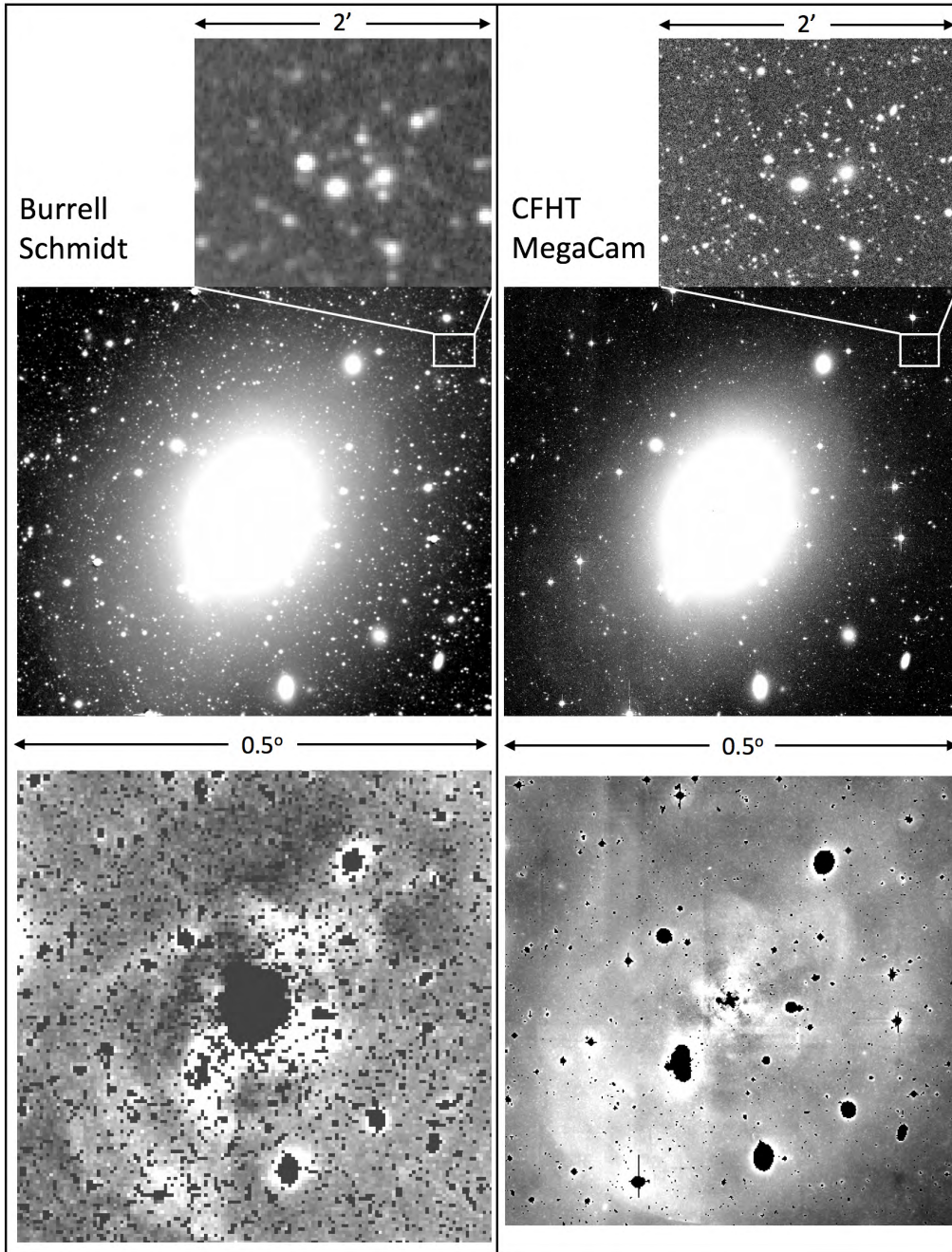


Figure 1. Deep imaging of the Virgo elliptical galaxy M49 from the 0.6/0.9m Burrell Schmidt (left, from [Janowiecki et al. 2010](#)) and the 3.5m CFHT (right, from [Arrigoni Battaia et al. 2012](#)) telescopes. The center images span 0.5° across, while the small images at the top show a $2'$ cutout of each image. The bottom images show the result of subtracting a smooth model for the M49 light, then masking bright pixels and spatially re-binning the images to show residual low surface brightness features.

of $\mu_{g,lim} \approx 28.5 - 29$ mag arcsec $^{-2}$. Complementary to these targeted surveys are new wide-area imaging surveys such as the *CFHT Legacy Survey* (Gwyn 2012), the *DECam Legacy Survey* on the CTIO 4m (Dey et al. 2019), and the *Hyper Suprime-Cam Subaru Strategic Program* on the 8.2m Subaru telescope (Aihara et al. 2018). Compared to targeted surveys, these wide-area surveys are somewhat shallower ($\mu_{r,lim} \approx 27.5-28.5$ mag arcsec $^{-2}$; Atkinson et al. 2013; Greco et al. 2018; Hood et al. 2018) but they cover hundreds to thousands of square degrees of the sky, enabling the study of LSB structures around large samples of galaxies spanning a wide range of physical environments.

The potential to push extraordinarily deep with large telescopes was demonstrated by Trujillo & Fliri (2016), who used the 10m GTC telescope to push down to a limit of $\mu_{r,lim} \approx 31.5$ mag arcsec $^{-2}$, albeit over only a small field of view ($< 5'$). Over larger areas such depths are not yet attainable, but looming on the horizon is LSST, whose 8.4m primary and 9.6 deg 2 camera will repeatedly image the night sky beginning in 2022. When completed, the main survey will deliver 825 dithered exposures of each patch of sky within its 18,000 deg 2 survey area. These dithered images will be critical for LSB science, not just for stacking to build signal, but also for identifying and removing scattered light in the imaging. While forecasting surface brightness depth is a dangerous game, if scattered light can be properly mitigated or modeled out of the data (see §4.1 below), LSST could potentially reach depths of $\mu_{g,lim} \approx 28$ mag arcsec $^{-2}$ in a single visit, and $\mu_{g,lim} \approx 31$ mag arcsec $^{-2}$ in a full stack of dithered images (Laine et al. 2018).

Space-based observatories offer advantages to LSB science as well, including more compact PSFs, lower sky backgrounds, and ultraviolet capabilities. Several deep optical imaging campaigns using *Hubble* have delivered rich datasets with the potential to reach very low surface brightness limits, such as the *Hubble Ultradeep Field* and its descendants (Beckwith et al. 2006; Koekemoer et al. 2013; Illingworth et al. 2013) and the *Hubble Frontier Fields* (Lotz et al. 2017). Recent work studying the diffuse light in Frontier Fields clusters (Montes & Trujillo 2014; Morishita et al. 2017; Montes & Trujillo 2018) and extended light of galaxies in the Ultradeep Field (Borlaff et al. 2019) have demonstrated that these datasets can reach limits as deep as $\mu \approx 31$ mag arcsec $^{-2}$ ($3\sigma, 3''$ scales). However, to fit in *Hubble's* small field of view, target galaxies and clusters must be at higher redshift, where cosmological surface brightness dimming makes the already-faint diffuse light around them even fainter. Fortunately, upcoming space missions such as *WFIRST* and *Euclid* will have much wider fields of view, potentially delivering LSB capabilities even for nearby galaxies and clusters. Greater gains may be possible through the development of space telescopes optimized for LSB imaging. One such example is the proposed MESSIER surveyor (Valls-Gabaud et al. 2017): a small (50cm) and fast ($f/2$) space telescope using a bi-folded Schmidt optical design to eliminate the extended PSF wings that normally arise from obscuration by the secondary (Muslimov et al. 2017). With a $2^\circ \times 4^\circ$ FOV and optimized to work in both optical and ultraviolet, MESSIER would conduct an all-sky survey probing diffuse starlight around galaxies, identifying the most diffuse galaxy populations, and tracing Ly α emission from the cosmic web.

3. Recent LSB Science Highlights

Here I highlight a handful of studies which demonstrate the state-of-the-art capabilities in LSB studies of diffuse light around galaxies and clusters. I concentrate on results gleaned from imaging in *integrated light*; additional *critical* information comes from spectroscopic data, studies of resolved stellar populations, and the properties of discrete tracers such as PNe and globular clusters, but will not be discussed here.

3.1. *Stellar Populations in Galaxy Outskirts*

The colors of the diffuse light surrounding galaxies provide important constraints on the stellar populations in their outer disks and halos. While broadband colors are a relatively crude tool for stellar population work, suffering from the well-known age-metallicity degeneracy, in the majority of cases they are the only means available for studying populations at low surface brightness. Compared to broadband imaging, spectroscopic studies become prohibitively difficult at extremely low surface brightness, while resolved star observations, perhaps the “gold standard” for studying stellar populations, are currently impractical beyond 10–15 Mpc. Because so much of our understanding of stellar populations is based on resolved star studies in the Local Volume, while studies of more distant galaxies must rely on imaging in integrated light, it is particularly important to cross-check inferences from the two techniques in galaxies where both are possible.

The halos of nearby spiral galaxies provide one such opportunity. Because their integrated light is dominated by old red giant branch stars, halo stellar populations are relatively simple and make for a clean test of the two techniques. But photometric accuracy in integrated light is critical; color uncertainties even as small as 0.1 mag can lead to significant uncertainty in the underlying populations. Indeed, some early work tracing the red colors of outer disks and halos were unduly influenced by the extended wings of the PSF scattering light outwards from the bright nuclei of the galaxies (see e.g. the discussion in Sandin 2014, 2015). However, recent studies do much better at constraining colors at low surface brightness. For example, deep imaging of the halo of NGC 4565 by Infante-Sainz et al. (in prep) achieves color uncertainties of $\lesssim 0.05$ mag at $\mu_r \approx 28$ mag arcsec⁻², and indicates metallicities in the range $[\text{Fe}/\text{H}] = -0.7$ to -1.7 . This compares favorably to the resolved star analysis of Monachesi et al. (2016), which derives a halo metallicity of $[\text{Fe}/\text{H}] = -1.2 \pm 0.3$ for fields at similar radii. The consistency in the inferred metallicity is promising, although the quality of the match is still sensitive to systematic details (such as the population age) in the modeling of the integrated colors.

A second test involves the star formation history in outer disks; here, the situation becomes more complex, as multiple stellar populations contribute to the integrated light. Nonetheless, significant headway can be made by folding in additional constraints. Deep imaging of the nearby spiral M101 by our group (Mihos et al. 2013, see Figure 2a) revealed the galaxy’s distorted outer disk extending nearly 50 kpc from the center. The very blue colors of the light ($B - V = 0.2 \pm 0.05$ at $\mu_B = 29.5$ mag arcsec⁻²), coupled with the lack of significant *GALEX* FUV emission, argued for a weak burst of star formation 250–350 Myr ago which has since largely died out. Subsequent *Hubble* imaging (Mihos et al. 2018) resolved multiple stellar populations (Figure 2b), including a discrete “lump” of stars in the blue helium burning sequence indicative of a coeval population evolving off the main sequence. Detailed stellar population models place the age of this population at 300–400 Myr, in excellent agreement with constraints from the integrated light. Of course, the resolved populations provide additional constraints as well, showing the stellar populations of the outer disk to be quite metal-poor, with $[\text{Fe}/\text{H}] = -1.15 \pm 0.2$.

The agreement between the resolved populations and integrated light in studies such as these give confidence in our ability to study stellar populations at low surface brightness. However, the number of galaxies in which these tests have been done is relatively small. As upcoming missions like *JWST*, *WFIRST*, and *Euclid* extend both the reach and scope of resolved population studies, and as more deep imaging of diffuse integrated light becomes available from existing telescopes and LSST, comparing these techniques in populations which span a wider range of environment and galaxy type will be particularly important.

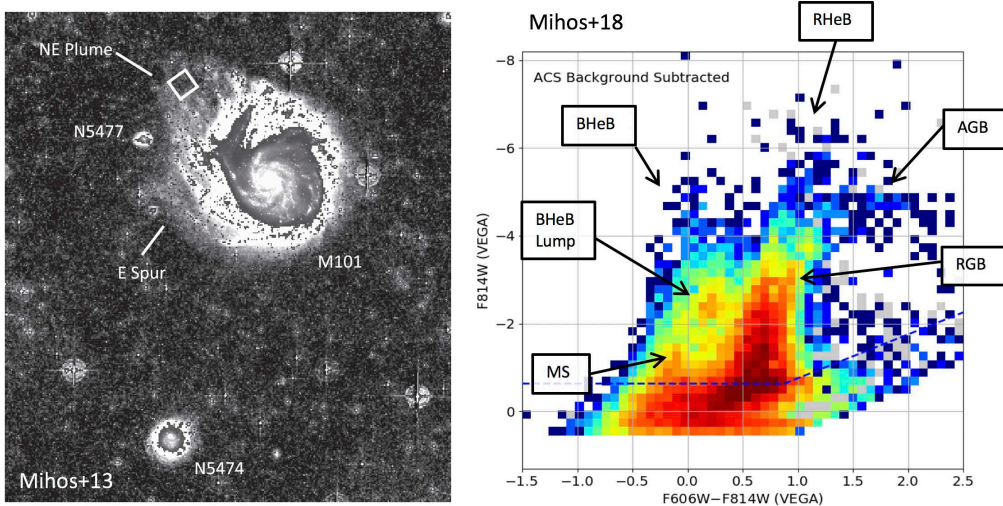


Figure 2. Left: Deep imaging of the spiral galaxy M101 showing the diffuse outer regions of the disk (Mihos et al. 2013). The white box in the NE Plume shows the location of our *Hubble* ACS imaging. Right: Color-magnitude diagram of stars in *Hubble* imaging, showing various stellar populations including a coeval lump of stars in the BHeB sequence. (Mihos et al. 2018).

3.2. Galaxy Accretion and the Structure of Stellar Halos

At sufficiently low surface brightness, the halos of galaxies should be filled with streams from accreted satellites. The morphologies of these streams are sensitive to properties of the accretion, such as mass and angular momentum of the satellite, and the time of accretion (Johnston 2016; Karademir et al. 2019). These events are well-traced by resolved star imaging of galaxies within 5 Mpc (e.g. Okamoto et al. 2015; Crnojević et al. 2016; McConnachie et al. 2018), and many more tidal streams have been found in the integrated light around more distant galaxies. (see, e.g., Martínez-Delgado 2019). As new wide-area surveys probe down to $\mu \approx 28$ mag arcsec $^{-2}$ and below, tidal streams can be detected around much larger samples of galaxies, studying the accretion properties of galaxies as a function of morphology, mass, color, and environment.

Traditionally, identification and classification of accretion events in deep imaging has largely been done by eye (e.g. Nair & Abraham 2010; Atkinson et al. 2013; Hood et al. 2018), as the low surface brightness and irregular structure of tidal streams makes them particularly challenging targets for automated detection algorithms. The quantity of data due in from new deep imaging surveys make this approach impractical; instead, new algorithms are needed to detect accretion signatures around much larger samples of galaxies. This is a challenging task. For example, while the algorithm of Kado-Fong et al. (2018) identified high-frequency substructure around galaxies, morphological *classification* of these structures still required human inspection. In contrast, Walmsley et al. (2019) have developed a neural network algorithm to both identify and classify tidal debris around galaxies in deep imaging but the technique is limited by the lack of comprehensive training samples. Ideally, algorithms would connect the morphology of the detected features back to the physical parameters of the accretion event: angular momentum, mass, accretion time, etc. Some progress on this front has been made by Hendel et al. (2019), who test automated morphology algorithms against controlled N-body simulations of accretion events. While all these techniques show promise, training and applying them across large and heterogeneous survey datasets remains a work in progress.

At even lower surface brightness, more information is available in galaxies’ diffuse stellar halos. First, many more tidal streams are thought to be found at or below $\mu_g \sim 29$ mag arcsec $^{-2}$ (Bullock & Johnston 2005); the bright streams found to date represent only the tip of the iceberg. Over time, these streams will mix spatially and become even more diffuse, but even once streams are lost as individual objects, simulations suggest that the structure of the smooth stellar halo remains sensitive to galaxies’ accretion properties, with steeper density profiles and metallicity gradients reflecting a quieter accretion history (Cook et al. 2016). However, tracing these halos requires imaging well below $\mu_g = 30$ mag arcsec $^{-2}$, an extremely challenging prospect for current imaging campaigns. Recently, Merritt et al. (2016) used Dragonfly imaging with characteristic depth $\mu_g \approx 29.5$ mag arcsec $^{-2}$ ($1\sigma, 1'$ scale) to search for halo light in a sample of nearby spirals. While azimuthal averaging erases spatial information in the imaging, it allows one to push to lower surface brightness, and the Merritt et al. analysis traced the azimuthally averaged surface brightness profiles down to $\mu_g \approx 30-32$ mag arcsec $^{-2}$ (2σ). At this level, the profiles suggest a wide range of inferred halo properties — including several galaxies with *no* detected halo light — and provide some tension with cosmological simulations of galaxy formation. But with only eight galaxies in the sample it is difficult to draw broad conclusions; a proper understanding of the structure and demographics of galaxy halos will require deeper imaging across much larger samples.

3.3. Intracluster Light

The diffuse intracluster light (ICL) that pervades galaxy clusters traces galaxy accretion over the largest scales. Mapping the ICL in nearby clusters like Virgo and Fornax is particularly important, because at this distance we have complementary information on ICL stellar populations and kinematics from discrete tracers such as RGB stars, planetary nebulae, and globular clusters. However, nearby clusters are large in angular size (Virgo’s core [virial] radius spans $\sim 2.1^\circ$ [5.4°]; Ferrarese et al. 2012) such that LSB imaging of these clusters demands deep *and uniform* imaging over very wide fields. Much of the core of Virgo (along with that of the M49 subgroup) was first imaged down to $\mu_V = 28.5$ mag arcsec $^{-2}$ by Mihos et al. (2005, 2017), with the whole 105 deg 2 virial area of the cluster subsequently imaged to comparable depths by the *Next Generation Virgo Survey* team (Ferrarese et al. 2012). In the south, the *Fornax Deep Survey* has mapped the diffuse light in Fornax (Iodice et al. 2016), although reflections from bright foreground stars complicate the imaging in many areas of the cluster.

These surveys, along with imaging of more distant clusters, have yielded a plethora of information about diffuse galaxy populations and ICL formation. The large low surface brightness galaxies first identified in Virgo by Sandage & Binggeli (1984) have been uncovered in large numbers in Coma (and re-dubbed “ultra-diffuse galaxies”; van Dokkum et al. 2015; Koda et al. 2015) and Fornax (Venhola et al. 2017), and are now detected at even fainter levels in Virgo (Mihos et al. 2005, 2017). Merging clusters show cluster-wide plumes of diffuse light (e.g. Feldmeier et al. 2004; Arnaboldi et al. 2012), evidence of rapid, on-going generation of ICL during cluster mergers. On smaller scales, faint streamers and shells in the halos of cluster ellipticals trace the tidal stripping of galaxies in the cluster environment (Janowiecki et al. 2010). The halos of massive Virgo and Fornax ellipticals have been imaged out beyond 100 kpc (e.g. Rudick et al. 2010; Mihos et al. 2013; Iodice et al. 2016); at these radii, the light become significantly bluer, indicative of younger and/or more metal-poor stellar populations where the halo begins to merge into the cluster’s diffuse ICL. The long, thin ICL streams in Virgo also have colors similar to those of low luminosity spheroidal galaxies in the cluster (Rudick et al. 2010), arguing that tidal shredding of faint galaxies is another important channel for ICL formation.

As clusters assemble, the fraction of light in the ICL is expected to grow, and its morphology will evolve as streams continually form and disrupt (Rudick et al. 2006). Imaging clusters at higher redshifts thus affords the possibility of tracking the evolution of ICL with time. Several recent studies have used the deep Hubble Frontiers Fields (Montes & Trujillo 2014; Morishita et al. 2017; Montes & Trujillo 2018) or CLASH (Burke et al. 2015; DeMaio et al. 2018) datasets to study ICL at redshifts $z \sim 0.3\text{--}0.8$. Here, imaging the ICL becomes *even harder* due to cosmological surface brightness dimming, but through careful background subtraction and masking of contamination, these studies trace the ICL out to 100 kpc and beyond, where its rest-frame surface brightness reaches $\mu_V \approx 26\text{--}27$ mag arcsec $^{-2}$. Strong color gradients are again seen in the transition region between the central galaxy and the ICL (Morishita et al. 2017; Montes & Trujillo 2018; DeMaio et al. 2018). Stellar population modeling of the ICL colors indicate populations which are both metal-poor *and* significantly younger than those in the central galaxy itself (Morishita et al. 2017; Montes & Trujillo 2018), suggesting that at these redshifts the ICL is actively growing via the accretion of star forming galaxies. However, there is still significant uncertainty about when the *bulk* of the ICL formed; some studies find significant evolution since $z \sim 0.5$ (Burke et al. 2015; Morishita et al. 2017), while others infer milder evolution (Guennou et al. 2012; Montes & Trujillo 2018), and the detection of diffuse light in the $z = 1.2$ cluster MOO J1014+0038 (Ko & Jee 2018) shows that at least some clusters have a significant ICL component in place quite early.

These studies paint a complex and sometimes contradictory picture where a variety of mechanisms contribute to ICL formation, including major mergers, tidal stripping, and galaxy destruction, but the relative amounts each process contributes, and the timescales on which they occur, are still only poorly constrained. Several problems contribute to this muddled picture. One is observational: because of surface brightness dimming, high- z observations often see only the *brightest* parts of the ICL, and miss a large fraction of the ICL at lower surface brightnesses. A second problem is definitional: there is no unambiguous metric for defining ICL, and different studies use different methods for determining the ICL fraction in clusters. When these different definitions are applied to simulated clusters (Puchwein et al. 2010; Rudick et al. 2011, see the discussion in Mihos 2015), depending on the metric chosen, the inferred ICL fraction varies by factors of 2–3 even within an individual cluster. Finally, there is the problem of progenitor bias: the massive clusters studied at $z \gtrsim 0.5$ are extreme overdensities, and not the progenitor population to local clusters such as Virgo and Fornax. To properly trace the evolution of ICL over time and across a range of cluster masses, careful attention will need to be paid to constructing proper comparison samples at low and high redshifts.

3.4. Narrowband Imaging of the Circumgalactic Medium

Just as deep broadband imaging has revealed the diffuse starlight around nearby galaxies, deep narrowband imaging has the potential to map the diffuse circumgalactic medium (CGM) surrounding these galaxies as well. This warm ionized gas lives at the boundary between galaxies and their extended environments and traces a variety of physical processes, including infall from the surrounding environment, the ejection of gas via AGN or starburst activity, and tidal stripping and shocking of gas. The CGM has been observed via Ly α emission around bright AGN and starburst galaxies in ground-based optical imaging and spectroscopy for high redshift systems, and from space-based UV imaging for objects at low redshift (see, e.g., Tumlinson et al. 2017). Detecting the CGM around more quiescent galaxies locally is challenging, however, as it requires narrowband imaging that is both wide and deep to survey the large angular scales around nearby galaxies.

Even in the strongest emission lines, the optical emission from the CGM is expected

to be extremely faint; for example, modeling of $H\alpha$ emission from the CGM at $z = 0$ (Lokhorst et al. 2019) suggests that pushing down to $\approx 10^{-19}$ to 10^{-20} $\text{erg s}^{-1} \text{cm}^{-2} \text{arcsec}^{-2}$ will be needed to detect this gas. While this is significantly deeper than current imaging capabilities, the CGM may have significant substructure (see e.g. simulations by Schaye et al. 2015; van de Voort et al. 2019) such that denser pockets of gas could be detectable at brighter thresholds. Indeed, this is borne out by recent deep $H\alpha$ imaging of M101 and M51 (Watkins et al. 2017, 2018), which reach a depth of 5×10^{-19} $\text{erg s}^{-1} \text{cm}^{-2} \text{arcsec}^{-2}$ (see Figure 3). A broad, 40 kpc long plume of diffuse $H\alpha$ is tentatively detected extending from the northeast edge of the galaxy’s disk, while M51 clearly shows a large ionized cloud just north of the system. The physical origin of these clouds is unclear, although their tentative association with tidal features in the galaxies suggest they may be gas tidally stripped from the disk and shock- or photo-ionized in the circumgalactic environment.

While observations such as these are intriguing, imaging an order of magnitude deeper to reach the more diffuse CGM may prove difficult. Aside from the obvious problem of fewer photons, several technical challenges arise in doing wide-field narrowband imaging. The fast beams which deliver the wide field of view and large pixel scale that normally help with LSB imaging become problematic when coupled with interference filters, widening the band pass and increasing the sky background. It is also more difficult to achieve low surface reflectivities on interference filters, leading to brighter reflections contaminating the imaging (see §4.1 below). Working in the red at $H\alpha$ introduces other problems as well, such as increased sky brightness from OH night sky lines and contamination due to CCD fringing. However, there are paths forward. Imaging bluer, at [OIII], alleviates the problems of fringing and OH lines in the red and results in quieter backgrounds (Mihos et al., in prep), although at the lowest metallicities [OIII] emission from the CGM will be suppressed. Additionally, new optical designs which put the interference filter at the telescope entrance (Lokhorst, this volume) could mitigate some of the complications that arise due to fast telescope beams. Whether these techniques prove sufficient to reach the truly diffuse emission from the extended CGM will be interesting to see.

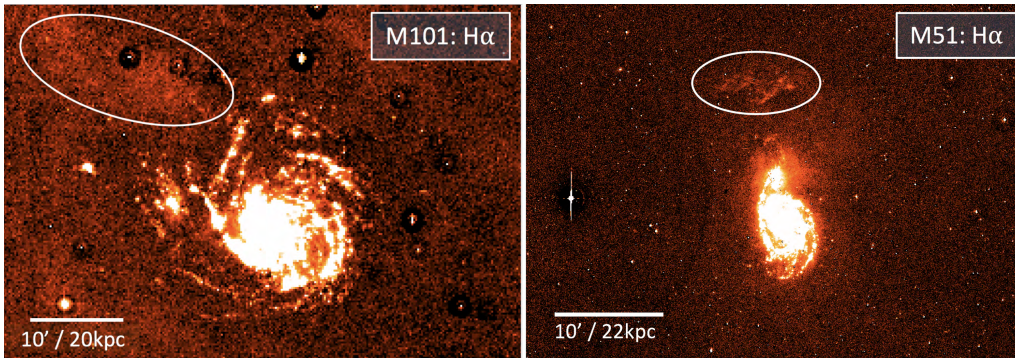


Figure 3. Deep $H\alpha$ imaging of M101 and M51 from Watkins et al. (2017, 2018, respectively), showing regions of extended diffuse $H\alpha$ emission in the outskirts of each system.

4. Challenges at Lower Surface Brightnesses

Extending the reach of deep LSB imaging to even lower surface brightness levels will present a number of challenges. The primary sources of uncertainty are systematic in nature, arising both from instrumental effects (stray light, flat fielding variations) and from astrophysical contamination (Galactic cirrus, foreground stars, faint background

sources). While the current LSB imaging techniques mitigate these effects down to $\approx 28\text{--}30$ mag arcsec $^{-2}$, pushing deeper will require even more stringent controls on these systematics. Here I highlight a few of the most concerning issues.

4.1. Internal Reflections

Bright objects in the field of view introduce scattered light across the image, due to the extended wings of the PSF and reflections between the CCD and various optical elements in the light path. The wings of the PSF are relatively simple to control, as they are radially symmetric, centered on the source, and do not vary appreciably as a function of source position on the image. Deep imaging of bright stars can be used to measure and model the extended PSF, and correct for its effect on the images (e.g. Slater et al. 2009; Sandin 2014, 2015; Trujillo & Fliri 2016). Mitigation of reflections is much more complicated, however.

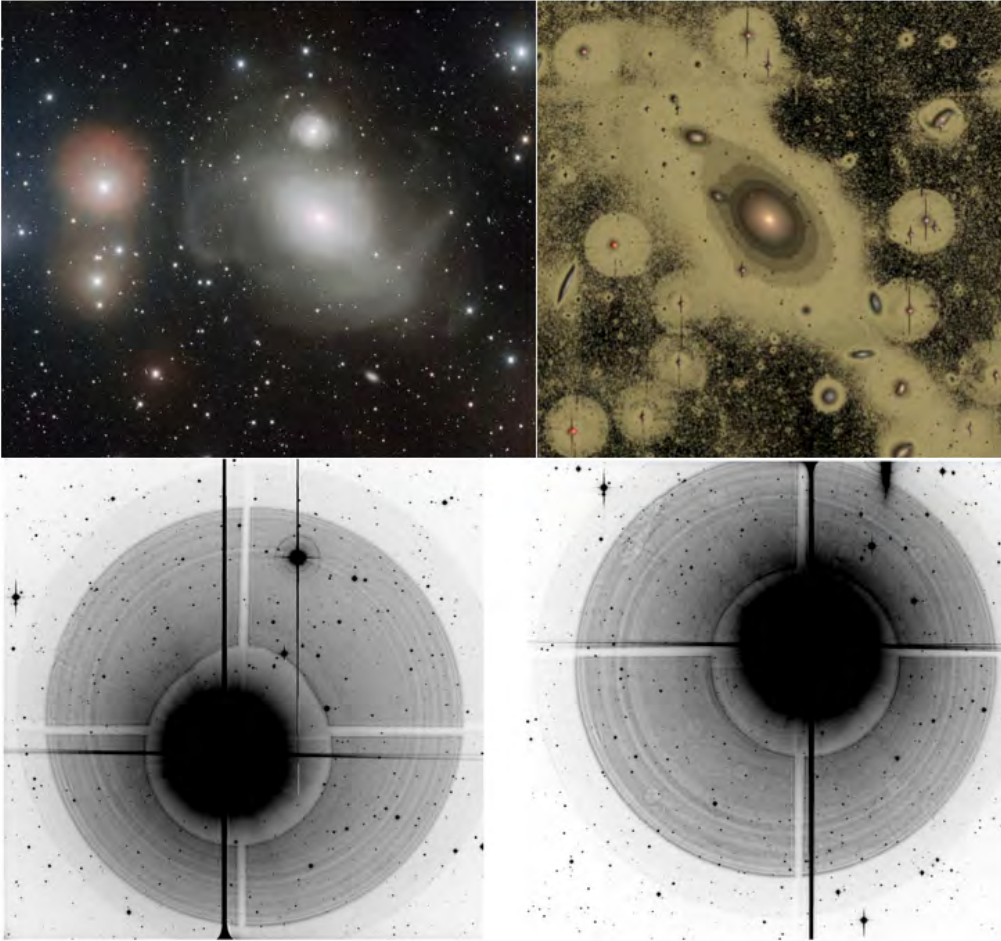


Figure 4. The impact of internal reflections. Top panels show reflections around bright stars in deep imaging from the VST (left) and CFHT (right) telescopes. The bottom panels show reflections in a 900s image of Arcturus ($V = -0.05$) taken with the Burrell Schmidt telescope (Slater et al. 2009), showing how the reflections shift when the star is moved to different positions in the field. The bright reflections in the VST and CFHT data are $\approx 3.5'$ in radius, while the faintest reflection visible in the Burrell Schmidt images is $19.5'$ in radius.

Examples of these reflections are shown in Figure 4. Since the most reflective surface in any optical camera is the CCD itself, these reflections arise from light reflecting off the CCD and the back down from the dewar window, filter, and any other optical element in the system. These reflections are radially asymmetric, and often have a complicated nested spatial structure due to bounces between differing elements. They are also typically off-center with respect to the source, with a position that changes relative to the source depending on position in the field. Finally, they have high frequency spatial structure that is virtually unmodelable, arising from surface variations on the optical elements, shadowing and scattering off of the secondary mirror support, and the spatially varying diffraction pattern of the telescope across the field of view.

These reflection halos around stars can also be quite large — extending to tens of arcminutes and beyond — and imprint complex low surface brightness patterns over large areas of the image. At current depths, these reflections can be minimized by the use of aggressive anti-reflective coatings, reducing the number of reflective elements in the system, modeling and subtracting reflections, and employing large scale dither-and-stack techniques to reduce the high frequency residuals (see *e.g.* Slater et al. 2009; Karabal et al. 2017). However, even in well-designed optical systems, these reflections become problematic at greater depths. For example, using the LSST scattered light model (LSST Science Collaboration et al. 2009), in LSST imaging, a 7th magnitude star will imprint a 40' diameter halo at 29.5 mag arcsec⁻², along with reflections stretching across the full 3.5° field of view at 31 mag arcsec⁻². This is for *one* 7th magnitude star; the full reflection pattern will be the sum of that imprinted by *all* stars across the field of view, of which, for LSST, there will be *many*. Compounding the problem is the fact that reflections are of course imprinted by all objects in the field, including the galaxies themselves, which turns the correction problem into one involving 2D deconvolution rather than simple subtraction. A full solution for characterizing these reflections and removing this scattered light from LSST imaging will require a significant investment of calibration time, computing resources, and work effort if the full LSB capabilities of the survey are to be realized.

4.2. Contamination from Galactic Cirrus

Another significant source of contamination in LSB imaging is the so-called “Galactic cirrus” arising from Milky Way starlight scattering off dust in the local interstellar medium. In deep optical imaging, this dust-scattered light creates a patchy and diffuse foreground screen, which can often mimic tidal structure (Cortese et al. 2010). This dust also radiates thermally in the infrared, and can be well-traced by deep infrared imaging. Cirrus is visible in the far ultraviolet as well, due to scattering of UV light by the dust (Witt et al. 1997; Boissier et al. 2015), along with some additional contribution from molecular hydrogen mixed in with the dust and fluorescing in the Lyman band (*e.g.* Sternberg 1989; Sujatha et al. 2010).

While Milky Way dust is thickest in the Galactic plane, tenuous cirrus exists even at high Galactic latitudes (Planck Collaboration et al. 2016) and is easily visible in deep optical imaging. Figure 5 shows imaging of the Virgo Cluster at optical, *Herschel* 250 μ m, and *GALEX* FUV wavelengths (from Mihos et al. 2017; Davies et al. 2010; Boissier et al. 2015, respectively). Even at $b = 75^\circ$, Virgo has significant contamination from dust at surface brightnesses of $\mu_V \approx 27$ mag arcsec⁻², visible in optical imaging as broad and diffuse streamers of light to the north, south, and southeast of M87 (near the center of the northern part of the optical image). These features are also seen in both the 250 μ m and FUV imaging, which show M87 and the Virgo core surrounded by a ring of cirrus. The multiwavelength data thus acts as a cross-check on the nature of the diffuse optical light:

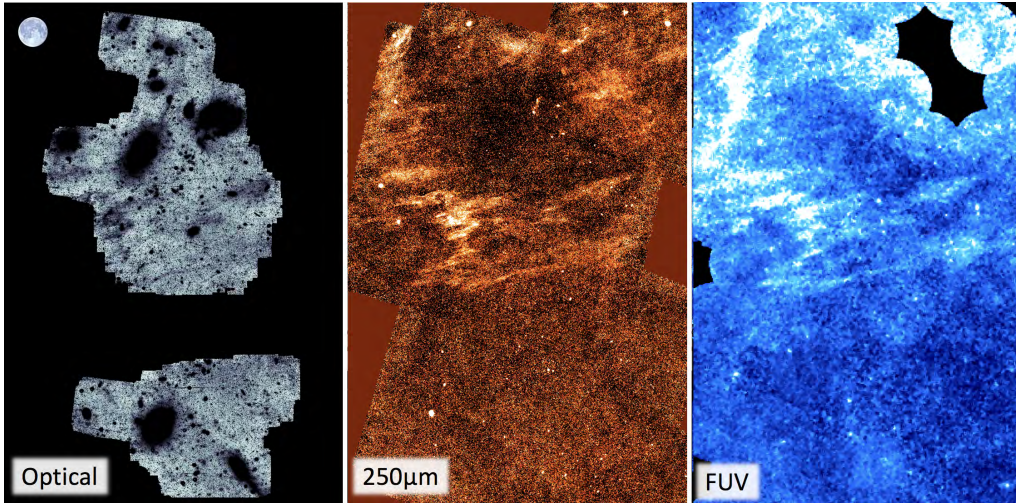


Figure 5. Deep imaging of the Virgo Cluster in optical, *Herschel* 250 μm , and *GALEX* FUV wavelengths (from Mihos et al. 2017; Davies et al. 2010; Boissier et al. 2015, respectively). The *Herschel* and *GALEX* data reveal emission from Galactic cirrus, tracing many features also seen in the diffuse optical light. North is up, east is to the left, and the Moon icon shows a 0.5 $^\circ$ scale.

features that lack FUV/IR emission are likely to be diffuse starlight around extragalactic sources. M87’s extended stellar halo and the tidal streams to the northwest are all clear of FUV/IR emission, as are the diffuse light features in the southern field around M49; all are bona-fide Virgo stellar light (Mihos et al. 2017).

Unfortunately, using the multiwavelength data to make a quantitative *correction* to optical imaging is much more problematic. There is rough linear correlation between IR emission and optical surface brightness in the Galactic cirrus (e.g. Witt et al. 2008), such that, given sufficiently deep IR data, one could try a “scale and subtract” approach to remove the cirrus (Mihos et al. 2017). However, the quality of this subtraction is quite variable; there is significant scatter in the IR-optical correlation, since the intensity of the scattered optical light and the thermal IR emission both depend on a wide range of parameters, such as the properties of the dust grains, the stellar populations illuminating the dust, and the relative spatial distribution of the dust with respect to the illuminating stars (e.g. Bianchi et al. 2017). Compounding the problem is the need for deep and high-spatial resolution IR imaging. While the targeted *Herschel* 250 μm imaging of Virgo shown in Figure 5 delivers good depth, the 18” beam size is a relatively poor match to arc-second optical resolution. The situation for other sight-lines through the Galaxy is worse. One is limited to all-sky far-IR data such as the reprocessed IRAS 100 μm maps (Miville-Deschênes, & Lagache 2005) or *Planck* dust maps (Planck Collaboration et al. 2016) which have 4–5’ resolution, or the mid-IR WISE imaging (Meisner & Finkbeiner 2014) which has better spatial resolution but contains a variety of large-scale background residuals that make it less reliable at the lower surface brightness. Alternatively, one can attempt to use the FUV maps to trace cirrus, but there can often be significant differences between the the FUV, IR, and optical maps, as seen in Figure 5. All these complications make the multiwavelength data useful as a qualitative signpost for cirrus contamination, but less helpful for actually removing the contamination.

At lower surface brightnesses the problem is likely to only get worse, as the sky coverage of Galactic cirrus increases rapidly at more diffuse levels. Scaling from the Planck Collaboration et al. (2016) dust map, roughly 10% of the sky is covered by cirrus with

thermal emission similar to that giving rise to the scattered optical light seen in Figure 5. The sky coverage increases to 80% for cirrus with diffuse IR emission a factor of 20 lower; under a simple linear scaling of the IR and optical flux, this would correspond to cirrus with an optical surface brightness of $\mu_V \approx 30\text{--}31 \text{ mag arcsec}^{-2}$. At this depth, with no deep, high-resolution IR data for guidance, disentangling cirrus contamination from extragalactic diffuse starlight will be extraordinarily hard. One possibility is to use the optical data itself: Román et al. (2019) show that the optical colors of the cirrus in SDSS Stripe 82 imaging are often distinct from that of extragalactic sources. If this result holds up more widely, and at even lower surface brightnesses, better discrimination may be possible. Nonetheless, correction for the contamination remains problematic, and cirrus-contaminated fields will likely remain a significant challenge for LSB science.

5. Looking Forward

At the end of our presentations, many of us in the LSB science community often conclude by saying “The future of low surface brightness science is bright!” While that is most certainly true, I can’t also help but think back the words of Stebbins & Whitford (1934) after tracing M31’s surface brightness so deeply some 85 years ago: “In fact, were it not for the interference of the field stars, the detection ... to 27 mag arcsec⁻² would really be easy.” Over the years, advances in imaging techniques have allowed astronomers to pierce that threshold, and we are now capable imaging diffuse light down into the 28–30 mag arcsec⁻² regime, with tantalizing hopes of going even deeper. To echo Stebbins & Whitford, if not for the issues of cirrus, scattered light, backgrounds, etc, the detection to 32 mag arcsec⁻² would really be easy. But it won’t be easy. We have not slain these dragons in our modern datasets, we have only driven them down into the lower depths of the noise. There they linger, lying in wait for us as we try to push deeper. So to *this* audience I say “The future of low surface brightness science is bright, but it’s also going to demand a lot of hard work.” Now let’s get to it.

Acknowledgements

I would like to thank my long-time collaborator Paul Harding for his continued technical wizardry with our Burrell Schmidt telescope, as well as the National Science Foundation, Research Corporation, the Mt Cuba Astronomical Foundation, and Case Western Reserve University for their support of our deep imaging work over the years.

Discussion

M. DISNEY: How do you envision the future in LSB imaging, both with ground- and space-based instruments?

C. MIHOS: What’s that old saying? “Making predictions is hard, particularly about the future.” Wide-area deep surface photometry is *so sensitive* to various systematic effects that going even deeper is going to take a lot of expensive, pain-staking work in the optical design, scattered light calibration, data reduction techniques, and correction for backgrounds and foregrounds. It’s unclear to me how well we’ll be able to do many of these things, or even how *committed* the broader astronomical community is to investing in this kind of effort. But there are a lot of smart people working hard on these issues, so I hope to be pleasantly surprised by progress over the coming years...

P.A. DUC: There is a fair correlation between the WISE 12 μ m emission and the cirri which could help mitigate their effects.

C. MIHOS: At brighter levels, yes, although the WISE imaging has a variety of optical ghosts and other large-scale background residuals that make it less reliable at lower surface brightnesses.

D. VALLS-GABAUD: Could an extremely accurate modelling of the full PSF across the FOV, and the ghosts produced (as done at the CFHT), be helpful in mitigating reflections, or we better design optical configurations which, by construction, have no reflections other than the ones at the surface of the CCD?

C. MIHOS: An accurate scattered light and PSF model will certainly help, although it can be very expensive in terms of ongoing calibration as it varies over the field of view and from filter to filter, and also can change over time. And of course the high frequency spatial structure of the scattered light will be essentially impossible to model. You are absolutely right that optical designs that reduce these effects will be particularly important — it's always better to eliminate contamination *before* it gets to the detector, rather than be forced to try and remove it in software after the fact.

S. DRIVER: We typically mask the reflections around stars down to quite faint magnitudes. Doesn't this eliminate most of the problem?

C. MIHOS: These reflections can be quite large, and at low surface brightness can cover scales of 0.5° or more on the imaging. We really don't want to be masking that much of our images as we try to push to lower surface brightness!

J. MURTHY: Some of the FUV emission from the Galaxy appears to arise from H_2 fluorescence, not from scattering from cirri.

C. MIHOS: That's really interesting, and could be part of the reason the structure of the cirrus can sometimes look significantly different between the FUV and IR imaging.

References

- Abraham, R. G., & van Dokkum, P. G. 2014, *PASP*, 126, 55
 Aihara, H., Arimoto, N., Armstrong, R., et al. 2018, *PASJ*, 70, S4
 Arnaboldi, M., Ventimiglia, G., Iodice, E., et al. 2012, *A&A*, 545, A37
 Arp, H., & Bertola, F. 1969, *Ap. Lett.*, 4, 23
 Arrigoni Battaia, F., Gavazzi, G., Fumagalli, M., et al. 2012, *A&A*, 543, A112
 Atkinson, A. M., Abraham, R. G., & Ferguson, A. M. N. 2013, *ApJ*, 765, 28
 Beckwith, S. V. W., Stiavelli, M., Koekemoer, A. M., et al. 2006, *AJ*, 132, 1729
 Bianchi, S., Giovanardi, C., Smith, M. W. L., et al. 2017, *A&A*, 597, A130
 Boissier, S., Boselli, A., Voyer, E., et al. 2015, *A&A*, 579, A29
 Borlaff, A., Trujillo, I., Román, J., et al. 2019, *A&A*, 621, A133
 Bullock, J. S., & Johnston, K. V. 2005, *ApJ*, 635, 931
 Burke, C., Hilton, M., & Collins, C. 2015, *MNRAS*, 449, 2353
 Capaccioli, M., Spavone, M., Grado, A., et al. 2015, *A&A*, 581, A10
 Cappellari, M., Emsellem, E., Krajnović, D., et al. 2011, *MNRAS*, 413, 813
 Cook, B. A., Conroy, C., Pillepich, A., et al. 2016, *ApJ*, 833, 158
 Cortese, L., Bendo, G. J., Isaak, K. G., et al. 2010, *MNRAS*, 403, L26
 Crnojević, D., Sand, D. J., Spekkens, K., et al. 2016, *ApJ*, 823, 19
 Davies, J. I., Baes, M., Bendo, G. J., et al. 2010, *A&A*, 518, L48
 DeMaio, T., Gonzalez, A. H., Zabludoff, A., et al. 2018, *MNRAS*, 474, 3009
 de Vaucouleurs, G. 1969, *Ap. Lett.*, 4, 17

- de Vaucouleurs, G., & de Vaucouleurs, A. 1970, *Ap. Lett.*, 5, 219
- Dey, A., Schlegel, D. J., Lang, D., et al. 2019, *AJ*, 157, 168
- Feldmeier, J. J., Mihos, J. C., Morrison, H. L., et al. 2004, *ApJ*, 609, 617
- Ferrarese, L., Côté, P., Cuillandre, J.-C., et al. 2012, *ApJS*, 200, 4
- Greco, J. P., Greene, J. E., Strauss, M. A., et al. 2018, *ApJ*, 857, 104
- Guennou, L., Adami, C., Da Rocha, C., et al. 2012, *A&A*, 537, A64
- Gwyn, S. D. J. 2012, *AJ*, 143, 38
- Hendel, D., Johnston, K. V., Patra, R. K., et al. 2019, *MNRAS*, 486, 3604
- Hood, C. E., Kannappan, S. J., Stark, D. V., et al. 2018, *ApJ*, 857, 144
- Illingworth, G. D., Magee, D., Oesch, P. A., et al. 2013, *ApJS*, 209, 6
- Iodice, E., Capaccioli, M., Grado, A., et al. 2016, *ApJ*, 820, 42
- Janowiecki, S., Mihos, J. C., Harding, P., et al. 2010, *ApJ*, 715, 972
- Johnston, K. V. 2016, in H.J. Newberg & J.L. Carlin (eds.), *Tidal Streams in the Local Group and Beyond*, ASSL Volume 420 (Switzerland: Springer), p. 141
- Kado-Fong, E., Greene, J. E., Hendel, D., et al. 2018, *ApJ*, 866, 103
- Karabal, E., Duc, P.-A., Kuntschner, H., et al. 2017, *A&A*, 601, A86
- Karademir, G. S., Remus, R.-S., Burkert, A., et al. 2019, *MNRAS*, 487, 318
- Ko, J., & Jee, M. J. 2018, *ApJ*, 862, 95
- Koda, J., Yagi, M., Yamanoi, H., et al. 2015, *ApJ*, 807, L2
- Koekemoer, A. M., Ellis, R. S., McLure, R. J., et al. 2013, *ApJS*, 209, 3
- Laine, S., Martinez-Delgado, D., Trujillo, I., et al. 2018, arXiv e-prints, [arXiv:1812.04897](https://arxiv.org/abs/1812.04897)
- Lokhorst, D., Abraham, R., van Dokkum, P., et al. 2019, *ApJ*, 877, 4
- Lotz, J. M., Koekemoer, A., Coe, D., et al. 2017, *ApJ*, 837, 97
- LSST Science Collaboration, Abell, P. A., Allison, J., et al. 2009, arXiv e-prints, [arXiv:0912.0201](https://arxiv.org/abs/0912.0201)
- Malin, D. F., & Carter, D. 1980, *Nature*, 285, 643
- Martínez-Delgado, D. 2019 in B. Montesinos, A. Asensio Ramos, F. Buitrago, R. Schdel, E. Villaver, S. Prez-Hoyos, I. Ordez-Etxeberria (eds.), *Highlights on Spanish Astrophysics X*, Proceedings of the XIII Scientific Meeting of the Spanish Astronomical Society, p. 146
- McConnachie, A. W., Ibata, R., Martin, N., et al. 2018, *ApJ*, 868, 55
- Meisner, A. M., & Finkbeiner, D. P. 2014, *ApJ*, 781, 5
- Merritt, A., van Dokkum, P., Abraham, R., et al. 2016, *ApJ*, 830, 62
- Mihos, J. C., Harding, P., Feldmeier, J., et al. 2005, *ApJ*, 631, L41
- Mihos, J. C., Harding, P., Spengler, C. E., et al. 2013, *ApJ*, 762, 82
- Mihos, C. 2015, IAU General Assembly 29, 2247903
- Mihos, J. C., Harding, P., Feldmeier, J. J., et al. 2017, *ApJ*, 834, 16
- Mihos, J. C., Durrell, P. R., Feldmeier, J. J., et al. 2018, *ApJ*, 862, 99
- Miville-Deschênes, M.-A., & Lagache, G. 2005, *ApJS*, 157, 302
- Monachesi, A., Bell, E. F., Radburn-Smith, D. J., et al. 2016, *MNRAS*, 457, 1419
- Montes, M., & Trujillo, I. 2014, *ApJ*, 794, 137
- Montes, M., & Trujillo, I. 2018, *MNRAS*, 474, 917
- Morishita, T., Abramson, L. E., Treu, T., et al. 2017, *ApJ*, 846, 139
- Muslimov, E., Valls-Gabaud, D., Lemaître, G., et al. 2017, *Applied Optics*, 56, 8639
- Nair, P. B., & Abraham, R. G. 2010, *ApJS*, 186, 427
- Okamoto, S., Arimoto, N., Ferguson, A. M. N., et al. 2015, *ApJ*, 809, L1
- Planck Collaboration, Ade, P. A. R., Aghanim, N., et al. 2016, *A&A*, 586, A132
- Puchwein, E., Springel, V., Sijacki, D., et al. 2010, *MNRAS*, 406, 936
- Román, J., Trujillo, I., & Montes, M. 2019, arXiv e-prints, [arXiv:1907.00978](https://arxiv.org/abs/1907.00978)
- Rudick, C. S., Mihos, J. C., & McBride, C. 2006, *ApJ*, 648, 936
- Rudick, C. S., Mihos, J. C., Harding, P., et al. 2010, *ApJ*, 720, 569
- Rudick, C. S., Mihos, J. C., & McBride, C. K. 2011, *ApJ*, 732, 48
- Sandage, A., & Binggeli, B. 1984, *AJ*, 89, 919
- Sandin, C. 2014, *A&A*, 567, A97
- Sandin, C. 2015, *A&A*, 577, A106
- Schaye, J., Crain, R. A., Bower, R. G., et al. 2015, *MNRAS*, 446, 521

- Schweizer, F., & Seitzer, P. 1988, *ApJ*, 328, 88
- Slater, C. T., Harding, P., & Mihos, J. C. 2009, *PASP*, 121, 1267
- Stebbins, J., & Whitford, A. E. 1934, Proceedings of the National Academy of Science, 20, 93
- Sternberg, A. 1989, *ApJ*, 347, 863
- Sujatha, N. V., Murthy, J., Suresh, R., et al. 2010, *ApJ*, 723, 1549
- Trujillo, I., & Fliri, J. 2016, *ApJ*, 823, 123
- Tumlinson, J., Peebles, M. S., & Werk, J. K. 2017, *ARAA*, 55, 389
- Valls-Gabaud, D., & MESSIER Collaboration 2017, in A. Gil de Paz, J.H. Knapen, & J.C. Lee (eds.), *Formation and Evolution of Galaxy Outskirts*, IAU Symposium 321, p. 199
- van de Voort, F., Springel, V., Mandelker, N., et al. 2019, *MNRAS*, 482, L85
- van Dokkum, P. G., Abraham, R., Merritt, A., et al. 2015, *ApJ*, 798, L45
- Venhola, A., Peletier, R., Laurikainen, E., et al. 2017, *A&A*, 608, A142
- Walmsley, M., Ferguson, A. M. N., Mann, R. G., et al. 2019, *MNRAS*, 483, 2968
- Watkins, A. E., Mihos, J. C., & Harding, P. 2015, *ApJ*, 800, L3
- Watkins, A. E., Mihos, J. C., & Harding, P. 2017, *ApJ*, 851, 51
- Watkins, A. E., Mihos, J. C., Bershad, M., et al. 2018, *ApJ*, 858, L16
- Welch, G. A., & Sastry, G. N. 1971, *ApJ*, 169, L3
- Witt, A. N., Friedmann, B. C., & Sasseen, T. P. 1997, *ApJ*, 481, 809
- Witt, A. N., Mandel, S., Sell, P. H., et al. 2008, *ApJ*, 679, 497
- Zwicky, F. 1952, *PASP*, 64, 242